

Passive Wireless Sensing Element for Sensitive Skin

Hiroyuki SHINODA and Hideki OASA

Department of Electrical & Electronic Engineering
Tokyo University of Agriculture and Technology
2-24-16 Koganei, Tokyo 184-8588 Japan
shino@cc.tuat.ac.jp and oasa@cc.tuat.ac.jp

Abstract

In this paper, we propose a method to realize flexible sensor skins integrated onto robot surfaces. By implanting wireless sensing elements in an elastic body, we obtain an elastic and tough sensitive skin which allows to be shaped freely. The element is a passive resonator chip whose resonant frequency reflects the stress around the chip. The resonant frequency is read out by a ground coil located at the bottom of the skin. The chip is simply composed of three functional parts, a coil for receiving and transmitting electrical power with wireless coupling, capacitance sensitive to stress, and ceramic resonator to provide high-Q resonance. The high quality factor brought by ceramic resonator enables us to distinguish a large number of chips, and to sense the stress with high accuracy. The structure, the method of wireless signal detection, and basic experiments of tactile sensing are presented.

1 Introduction

In order to realize practical robots working in unstructured and unpredictable surroundings with humans, we are facing a new problem of tactile sensing. That is how to give an elastic and tough sensor skin (sensitive skin) to the entire surface of a robot with a complex shape. For this purpose, any tactile sensing method reported so far[1, 2] has one or more defects of inelasticity, fragility, impracticable complicity of fabrication. In a pioneering work of an entire body perception, an interesting idea of sensing suit[3] was proposed. The sensing fabric is more flexible than a film-type sensor[5], but the instability of electrical contact among strings is difficult to avoid. Polymer electronics[4] is a hope, but it is not at a practical level yet now. From past methods, we find that those defects come from the wiring. If we can place small sensing elements in an elastic body without wiring, the skin will be tough and elastic as well as easy to fabricate in a free shape. Based on this consideration, we recently proposed a method called “telemetric

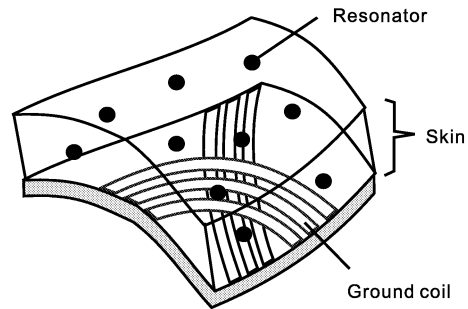


Figure 1: Basic concept of wireless tactile sensing.

skin”[6], and showed a sensing chip receiving electrical power and transmitting tactile signal by inductive coupling. In that research, the signal was produced by an integrated circuit on the sensing chip. Therefore it yields easy development into a multi-functional sensing chip. Meantime, we are afraid the cost might be too high for a practical use, especially at the early stage. In this paper we propose a new wireless tactile sensing device. Signal transmission based on inductive coupling between sensing chips and a ground coil, is the same as the former telemetric skin. The new component is that the sensing chip is composed of only passive components without transistors. The structure is simple, nevertheless each chip gives highly accurate digital signal representing the pressure around the chip.

2 Principle of Wireless Tactile Sensing

The basic concept of wireless tactile sensing is shown in Fig. 1 and 2. If we have a resonator which has some electromagnetic interaction with the ground coil located at the bottom of the skin, and whose resonant frequencies are sensitive to the stress around it, the resonator can be a wireless tactile sensing chip. A simple LC resonator as shown in Fig. 2, whose capacitance is stress-sensitive, is an example of it. The resonant frequency shift to reflect the stress is obtained wirelessly, by inductive excitation and observation of the relaxation with a

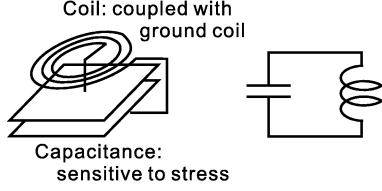


Figure 2: A simple example of tactile resonator to explain the concept of wireless tactile sensing.

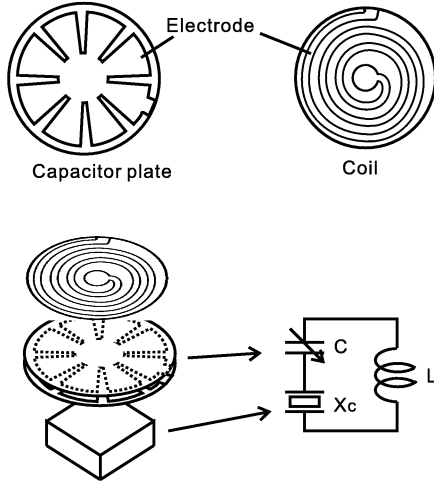


Figure 3: The sensing resonator proposed here. The radial cut of the sensing capacitor electrode is for preventing induction current which interferes the coupling between the chip coil and the ground coil.

ground coil. We obtain a stress distribution by detecting resonant frequencies of multiple chips sequentially.

A desirable resonator has high accuracy, quick response, and low cross-talk with other resonators having close resonant frequencies. For obtaining high accuracy and low cross-talk, the resonator must have high Q (quality factor). In order to obtain quick response without losing the accuracy and the low cross-talk, the resonant frequency must be as high as possible. Therefore a simple LC resonator is not proper for this tactile chip because the Q is less than 100 at frequencies higher than, for example, 1 MHz.

Other than LC resonance, several resonant phenomena are known. One is acoustic resonance. Resonance of quartz has both very high Q ($\sim 10^5$) and high resonant frequency. Ceramic resonator also has high Q (over 10^3). A surface acoustic wave (SAW) device can have high Q up to 10^4 , besides, the resonant frequency and quality factor are controllable by patterning of two dimensional electrode [8]. Another interesting resonance is NMR (nuclear magnetic resonance), but the signal is too weak to use in practical tactile sensing.

3 Structure of Sensing Chip

In this paper we propose a sensing resonator as shown in Fig. 3. The chip is composed of three functional parts, a coil L for receiving and transmitting electrical power, capacitance C which is sensitive to stress, and ceramic resonator X_C to provide high-Q resonance. Fabrication process of these parts has been well established.

A sensing chip based on SAW device [8] instead of C and X_C will be another challenging method. It is attractive that we can use not only frequency but also signal delay to distinguish a large number of chips [7]. However, we have to increase the operating frequency over 1 GHz to make the chip size smaller than several mm. Therefore we examine another sensing chip using C and X_C as shown in Fig.3.

Equivalent circuit of ceramic resonator is illustrated in Fig. 4 (a). The ceramic resonator has both a zero and a pole. The reactance of the serial connection of L, C and X_C is shown in Fig. 4 (b) and (c). The resonant frequency to maximize the circuit current in Fig. 3 is the frequency at which the following reactance

$$X = X_C + \omega L + \frac{1}{\omega C} \quad (1)$$

becomes zero. In a simple LC resonator, the large resistance contained in L results in a low quality factor. But in this L-C- X_C resonator, the equivalent inductance L_0 in X_C can be much larger than L, which brings higher quality factor than that of the simple LC.

Sensing is done by C. We can calculate the sensitivity, neglecting ωL , as

$$\frac{\Delta F_r}{F_r} = - \left(\frac{1}{1 + C_1/C} \cdot \frac{1}{1 + (C + C_1)/C_0} \right) \frac{\Delta C}{C}. \quad (2)$$

Therefore if C is comparable to C_0 and C_1 , the frequency change rate is comparable to the change rate of C. The resistance of the serial connection of C and X_C at F_r is given as

$$\text{Re}[X(f = F_r)] = \left(1 + \frac{C_1}{C} \right)^2 R_0. \quad (3)$$

Thus, the equivalent resistance increases by attaching C. This means a smaller C than C_1 weakens the signal amplitude. It will be informative to show typical parameters of a commercial resonator. In a 8 MHz resonator (Murata, Ceralock), $L_0 = 68 \mu\text{H}$, $C_0 = 6.4 \text{ pF}$, $R_0 = 4.5 \Omega$, and $C_1 = 39.6 \text{ pF}$.

4 Signal Intensity and Chip Design

Schematic diagram of signal detection is shown in Fig. 5. First we give the ground coil a burst current I_{in} as shown in Fig. 5 (b) to excite a chip. After

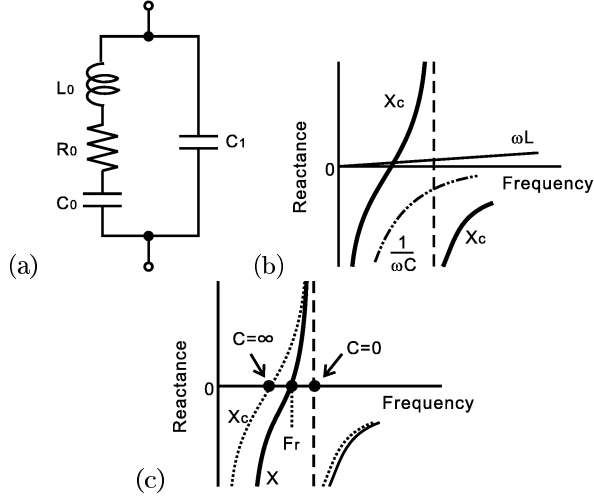


Figure 4: (a): Equivalent circuit of quartz and ceramic resonator X_C . (b): Illustrating reactance of L , C and X_C . (c): The reactance X of the serial connection of L , C and X_C . The resonant frequency F_r is the zero.

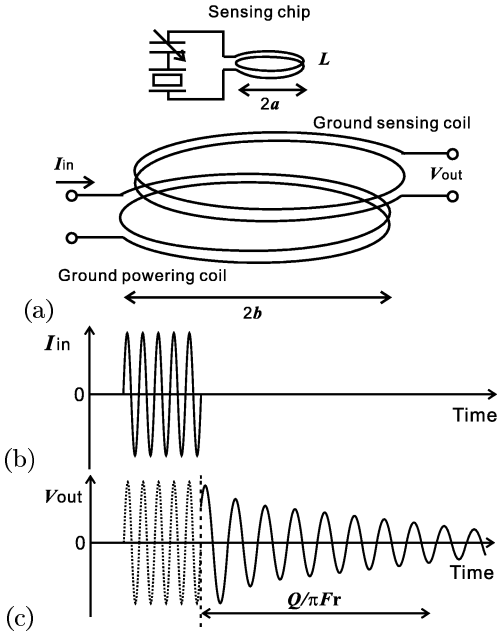


Figure 5: Schematic diagram of resonant frequency sensing. We observe the output voltage V_{out} by an input burst signal I_{in} .

stopping I_{in} , we observe the output voltage of another ground coil driven by the excited resonator. (It is also possible we use only one coil for both excitation and observation.) The frequency of output voltage is always the resonant frequency F_r regardless of the excitation frequency, but the amplitude is maximized when the excitation frequency is equal to F_r . The signal decays with time constant $Q/\pi F_r$. As we show in next section,

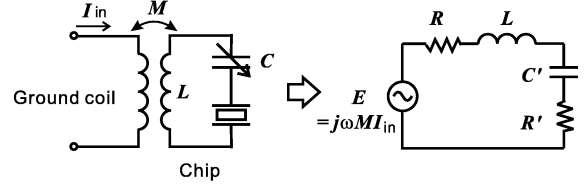


Figure 6: Equivalent circuit for understanding the resonant current at the chip coil L .

we measure the frequency of this signal.

Next we examine the theoretical signal intensity. In Fig. 6, the R is the equivalent resistance contained in the coil L at the resonant frequency. The C' and R' represent the impedance of the serial connection of C and X_C at the resonant frequency. When L is sufficiently small, the R' is approximated as Eq. (3).

Assume a chip coil with radius a and turn n is located at the center of the circular ground coil which has radius b and turn n_G . Then the mutual inductance M between them is written as

$$M = \mu_0 \frac{\pi a^2}{2b} n_G n \quad (4)$$

where μ_0 is the vacuum permeability. Therefore the observed voltage V_{out} is given as

$$V_{out} = \frac{\omega^2 M M'}{R + R'} I_{in} = \left(\frac{\pi \mu_0}{2b} \right)^2 \frac{\omega^2 a^4 n^2}{R + R'} n_G n' I_{in} \quad (5)$$

where M' is the mutual inductance between the chip coil and the ground sensing coil, and n'_G is the turn of the ground sensing coil.

For example, when $\omega = 10 \text{ MHz} \times 2\pi$, $a = 2 \text{ mm}$, $b = 5 \text{ cm}$, $n_G = n'_G = n = 5$, and $R + R' = 10 \Omega$, Eq. (5) is calculated into

$$V_{out} [\text{V}] = 0.006 I_{in} [\text{A}]. \quad (6)$$

At a low frequency, Eq.(5) tells us that the observed voltage is proportional to the square of the chip-turn n when $R < R'$. But in our experiments up to 40 turns at 10 MHz (for chip coil radius 2 mm, by 50 μm radius wire), the output voltage did not increase where $n > 10$, because the R increased at a comparable rate [9].

5 Frequency Detection

Figure 7 shows the procedure of resonant frequency detection. A digital-based circuit brings easy detection of multi-mode resonance. After we mold the sensor skin, the computer scans over the total bandwidth of all resonators, for obtaining rough estimate of each resonant frequency from the peak frequency. Using these recorded initial frequencies, we detect the precise resonant frequencies of chips one by one as follows.

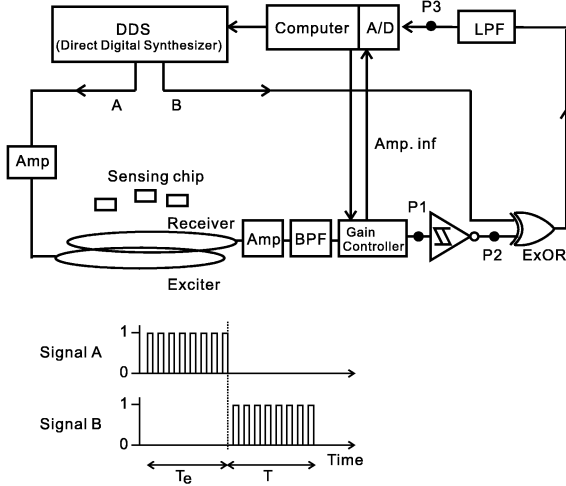


Figure 7: Block diagram of resonant frequency detection. Signal A excites the chip for T_e , and signal B is used for a reference signal.

One primitive method is counting the alternation of relaxation signal. To obtain the highest accuracy, we excite each chip during $T_e \sim Q/F_r$ and observe the relaxation signal during $T \sim Q/F_r$. The frequency error ΔF_r is given as

$$\frac{\Delta F_r}{F_r} = \frac{1}{TF_r} = \frac{1}{Q}. \quad (7)$$

For example, let F_r and Q be 10 MHz and 1000, respectively. If we assign 0.1 MHz bandwidth, that is, 1 % of 10 MHz for each chip, the dynamic range is 10^1 , that is about 3 bits.

The method to obtain higher frequency resolution is to measure the period of the signal more precisely, as we have a-priori knowledge that the signal has a single frequency. After shifting the signal frequency to a lower frequency through multiplication with a reference signal, we obtain its period from the waveform, which gives more precise signal frequency as follows. The block diagram in Fig. 7 illustrates the procedure. The received signal goes through a band-pass filter whose pass-band covers total bandwidth of all resonators. And after converting to a one bit signal as shown in Fig. 8, we take exclusive-OR with the reference signal. After low-pass filtering, we get the analog waveform $g(t)$ into a computer. The frequency of the waveform $g(t)$ is equal to the difference between the reference signal and the received signal.

The period of $g(t)$ is calculated from zero-crossings of a filtered signal $g*\phi(t)$ where $\phi(t)$ is a quasi-Gaussian kernel

$$\phi(t) = \begin{cases} \exp\{-\beta(t/T_1)^2\} \sin(\omega_0 t) & (|t| < T_1) \\ 0 & (|t| > T_1) \end{cases} \quad (8)$$

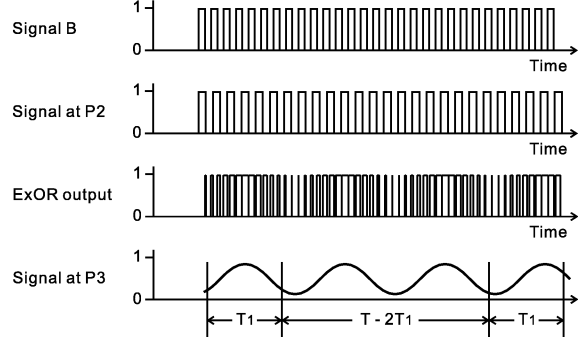


Figure 8: Illustration of processed signals. The frequency difference between the driving signal (signal B) and the detected signal (signal at P2) is obtained from the waveform at P3.

The parameter ω_0 is a rough estimate of frequency of $g(t)$, and we choose $\beta = 4.0$ to make the envelope smooth. We obtain the signal period from the zeros of $g * \phi(t)$ in $[T_1, T - T_1]$ excluding both ends of T_1 data. (Here the best estimate is obtained when $T_1 = T/6$. The proof omitted.)

Then the accuracy of frequency detection by this method is given as

$$\frac{\Delta F_r}{F_r} = \frac{n_d \sqrt{F_r}}{(TF_r)^{1.5} A} = \frac{N}{(TF_r)^{1.5} A} > \frac{N}{Q^{1.5} A}, \quad (9)$$

where A and n_d are the signal amplitude and the noise density at the signal frequency, respectively, at point P1 before digital operation in Fig. 7. The $N = n_d \sqrt{F_r}$ is the amplitude of an imaginary noise with a constant density n_d up to F_r . (The proof omitted.) If the SN ratio is 10 dB for such a white noise, the resolution is improved 100 times compared with Eq. (7), for the same data length T .

6 Experiment

We fabricate two prototypes of sensing chip, and examine the theory. One operates at 900 kHz, and the other one is a practical 8 MHz chip. In both chips, the sensing capacitor is made of two copper plates with oxidized surface facing each other. Sensitivity to pressure is given by natural unevenness of the plates. Though the shape of the chip is a circle in Fig. 3 to avoid stress concentration, here we fabricate the sensing capacitor in a square shape for convenience. The coil L is made of wire 0.1 mm in diameter. The dimension of each part is summarized in Table 1. The size of the ceramic resonators described in the table, is not that of the resonator itself, but that of the package. Except for L , we can miniaturize them without losing sensing ability. In

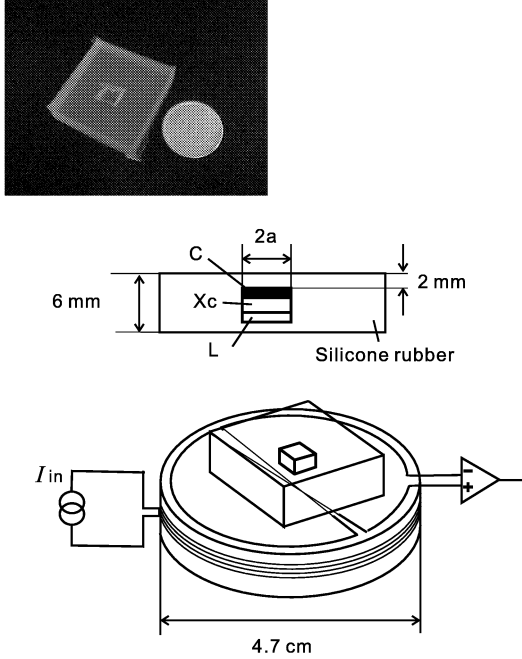


Figure 9: Experimental setup. We observe the resonant frequency of the sensing chip while we push on the silicon rubber surface.

Table 1: Structure and dimension of sensing chips.

	900 kHz	8 MHz
L	100 turns, $a = 4.2$ mm	5 turns, $a = 2.2$ mm
C	62 pF $7 \times 7 \times 0.5$ mm	23 pF $5 \times 5 \times 0.5$ mm
X_C	895 kHz $6 \times 5 \times 2$ mm	7.98 MHz $4.5 \times 4 \times 1.6$ mm

900 kHz operation, we need many turns for signal intensity, as is shown in the theory. And a low frequency chip is slow in response. Therefore it is not practical, however we fabricate it at first for obtaining reference data.

6.1 Results of the 900 kHz chip

Fig. 10 (a) shows an output signal with no sensing chip. Only driving signal is observed. The input current I_{in} is 6 mA in effective value. Fig. 10 (b) is a signal from the sensing chip at the resonant frequency. The resonance is observed. Here the output voltage is amplified 12000 times. In this basic experiment, the BPF (band-pass-filter) in Fig. 7 is not inserted. The effective noise value is 0.2 V. The waveform at point P3 in Fig. 7 is shown in Fig. 10 (c). We estimate the frequency from the data during $T = 512 \mu\text{s}$ with 1 MHz sampling. The plots in Fig. 11 are the detected frequencies through this procedure. When we

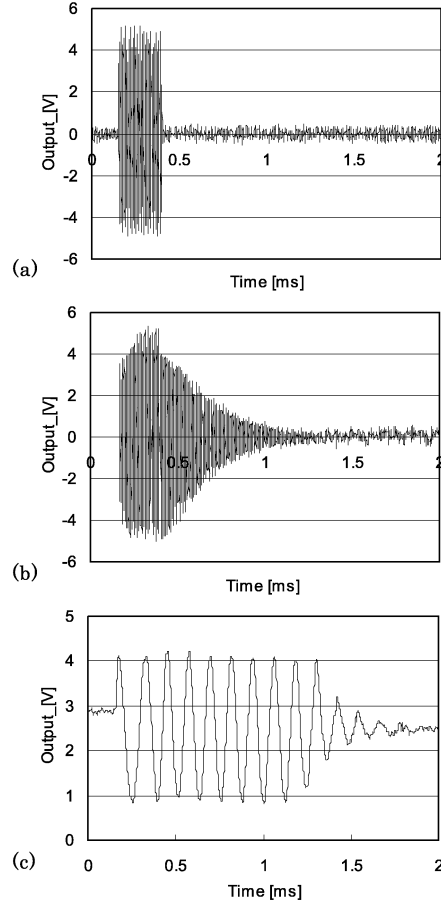


Figure 10: Experimental results of the 900 kHz chip. (a): Signal V_{out} with no sensing chip, at P1 in Fig. 7. (b): Resonance signal. (c): low-passed ExORed signal at P3. The driving current I_{in} is 6 mA.

pressed the sensor surface using a plastic cylinder with a radius of 5 mm, the resonant frequency changed. The standard deviations of the frequency detection are plotted on the identical figure. They were estimated from 100 measurements under an identical condition. These plots show the error is smaller than 20 Hz for 0.5 ms observation. The error ratio

$$\frac{\Delta F_r}{F_r} = 20/900,000 = 2 \times 10^{-5} \quad (10)$$

corresponds to the calculation of Eq. (9) when $F_r T = 450$, and SN ratio = 20 dB.

6.2 Results of 8 MHz chip

The experimental setup is unchanged from the previous one. Also in this experiment, the preliminary band-pass-filter is not inserted. Fig. 12 shows the detected signal. The input current I_{in} is 1 mA in effective value. The signal intensity 0.5 V corresponds to the calcula-

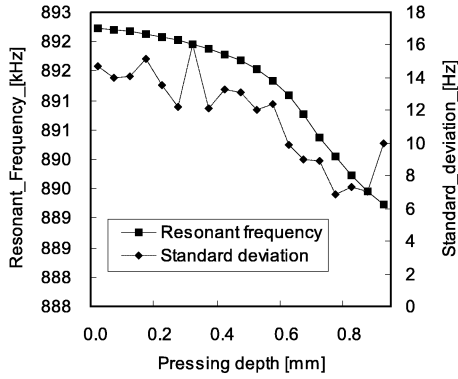


Figure 11: Experimental results of the 900 kHz chip. Measured resonant frequencies and their errors while we pressed the sensor surface. The data length used for the frequency estimation is $512 \mu\text{s}$.

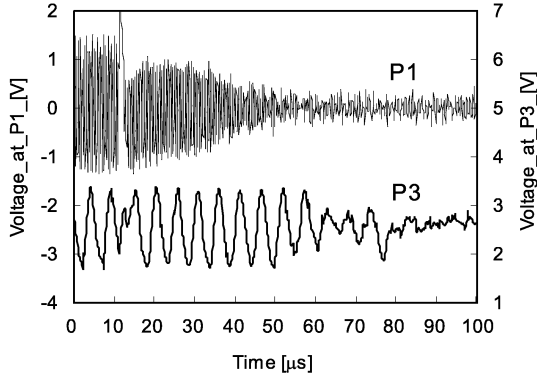


Figure 12: Experimental results of the 8 MHz chip. Signal V_{out} at point P1 in Fig. 7, and the signal at P3. The driving current I_{in} was 1 mA.

tion of Eq. (5) when we substitute 12Ω for $R + R'$. In this case, the signal amplitude was 0.5 V in effective value, to 0.2 V noise. When we pressed the sensor surface, the resonant frequency changed as shown in Fig. 13. The data length used for determining the frequency is $T = 20 \mu\text{s}$. The standard deviation was 1 kHz. The error ratio

$$\frac{\Delta F_r}{F_r} = 1\text{kHz}/8\text{MHz} \sim 1 \times 10^{-4} \quad (11)$$

corresponds to the calculation of Eq. (9) when $F_r T = 160$, and SN ratio = 10 dB.

Through this experiment, we could realize a sensing chip whose bandwidth was 30 kHz with 1 kHz resolution. The time needed to get one chip signal was shorter than $100 \mu\text{s}$. In calculation, 100 sensing chips whose initial frequencies span from 10 MHz to 20 MHz with 100 kHz interval, can be measured within 10 ms.

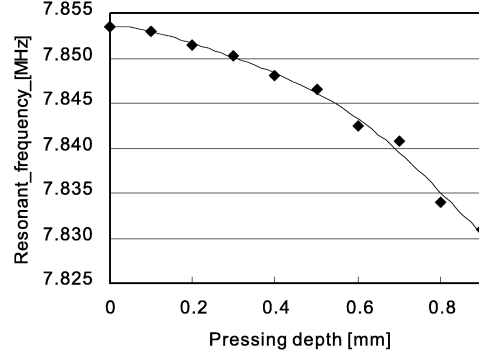


Figure 13: Experimental results of the 8 MHz chip. Measured resonant frequencies while we pressed the sensor surface using a plastic cylinder with a radius of 5 mm. The standard deviation was 1kHz. The data length used for frequency estimation is $20 \mu\text{s}$.

Acknowledgments

The research was partly supported by JSPS-RFTF 96P00801, the Japan Society for the Promotion of Science.

References

- [1] H. R. Nicholls and M. H. Lee, "A survey of robot tactile sensing technology," *Int. J. Robotics Research*, Vol. 8, No. 3, pp. 3 – 30, 1989.
- [2] M. H. Lee and H. R. Nicholls, "Tactile sensing for mechatronics - a state of the art survey," *Mechatronics*, Vol.9, No.1, pp.1-31, 1999.
- [3] M. Inaba, Y. Hoshino, K. Nagasaka, T. Ninomiya, S. Kagami, and H. Inoue, "A full-body tactile sensor suit using electrically conductive fabric and strings," *Proc. IEEE/RSJ IROS 96*, Osaka, pp. 450-457, 1996.
- [4] J. D. Madden, S. R. Lafontaine, and I. W. Hunter, "Fabrication by electrodeposition: building 3D structures and polymer actuators," *Proceedings - Micro Machine and Human Science 95*, Nagoya, Japan, 1995.
- [5] F-SCAN System. Tekscan Inc., MA, USA, 1997.
- [6] M. Hakozaki, H. Oasa and H. Shinoda, "Telemetric robot skin," *Proc. 1999 IEEE Int. Conf. on Robotics and Automation*, pp. 957-961, 1999.
- [7] A. Pohl, "A low-cost high-definition wireless sensor system utilizing intersymbol interference," *IEEE Trans. On Ultrasonics, Ferroelectrics, and Frequency Control*, Vol. 45, pp.1355, 1998.
- [8] A. Pohl, G. Ostermayer, and F. Seifert, "Wireless sensing using oscillator circuits locked to remote high-Q SAW resonators," *IEEE Trans. on Ultrasonics, Ferroelectrics and Frequency Control*, Vol.45, No.5, pp.1161-1168, 1998.
- [9] M. R. Shah, R. P. Phillips, R. A. Normann: "A study of printed spiral coils for neuroprosthetic transcranial telemetry applications," *IEEE Trans. on Biomedical Engineering*, Vol .45, No .7, pp.867-876, 1998.